



Article

Zymosan Particle-Induced Hemodynamic, Cytokine and Blood Cell Changes in Pigs: An Innate Immune Stimulation Model with Relevance to Cytokine Storm Syndrome and Severe COVID-19

Gábor Kökény^{1,2} , Tamás Bakos³, Bálint András Barta⁴, Georgina Viktória Nagy⁴, Tamás Mészáros^{3,5}, Gergely T. Kozma^{3,5}, András Szabó⁶, János Szebeni^{1,3,5,7,8,*}, Béla Merkely^{4,†} and Tamás Radovits^{4,†}

¹ Department of Translational Medicine, Semmelweis University, 1089 Budapest, Hungary

² International Nephrology Research and Training Center, Semmelweis University, 1089 Budapest, Hungary

³ Nanomedicine Research and Education Center, Department of Translational Medicine, Semmelweis University, 1089 Budapest, Hungary

⁴ Heart and Vascular Center, Semmelweis University, 1122 Budapest, Hungary

⁵ SeroScience Ltd., 1089 Budapest, Hungary

⁶ 2nd Department of Pediatrics, Semmelweis University, 1085 Budapest, Hungary

⁷ Department of Nanobiotechnology and Regenerative Medicine, Faculty of Health Sciences, Miskolc University, 2880 Miskolc, Hungary

⁸ Translational Nanobioscience Research Center, Sungkyunkwan University, Suwon 16419, Republic of Korea

* Correspondence: szebeni.janos@med.semmelweis-univ.hu or jszebeni2@gmail.com

† These authors contributed equally to this work.



Citation: Kökény, G.; Bakos, T.; Barta, B.A.; Nagy, G.V.; Mészáros, T.; Kozma, G.T.; Szabó, A.; Szebeni, J.; Merkely, B.; Radovits, T. Zymosan Particle-Induced Hemodynamic, Cytokine and Blood Cell Changes in Pigs: An Innate Immune Stimulation Model with Relevance to Cytokine Storm Syndrome and Severe COVID-19. *Int. J. Mol. Sci.* **2023**, *24*, 1138. <https://doi.org/10.3390/ijms24021138>

Academic Editor: Rob J. Vandebriel

Received: 31 October 2022

Revised: 9 December 2022

Accepted: 3 January 2023

Published: 6 January 2023

Abstract: Hemodynamic disturbance, a rise in neutrophil-to-lymphocyte ratio (NLR) and release of inflammatory cytokines into blood, is a bad prognostic indicator in severe COVID-19 and other diseases involving cytokine storm syndrome (CSS). The purpose of this study was to explore if zymosan, a known stimulator of the innate immune system, could reproduce these changes in pigs. Pigs were instrumented for hemodynamic analysis and, after i.v. administration of zymosan, serial blood samples were taken to measure blood cell changes, cytokine gene transcription in PBMC and blood levels of inflammatory cytokines, using qPCR and ELISA. Zymosan bolus (0.1 mg/kg) elicited transient hemodynamic disturbance within minutes without detectable cytokine or blood cell changes. In contrast, infusion of 1 mg/kg zymosan triggered maximal pulmonary hypertension with tachycardia, lasting for 30 min. This was followed by a transient granulopenia and then, up to 6 h, major granulocytosis, resulting in a 3–4-fold increase in NLR. These changes were paralleled by massive transcription and/or rise in IL-6, TNF-alpha, CCL-2, CXCL-10, and IL-1RA in blood. There was significant correlation between lymphopenia and IL-6 gene expression. We conclude that the presented model may enable mechanistic studies on late-stage COVID-19 and CSS, as well as streamlined drug testing against these conditions.

Keywords: cytokine storm; pulmonary hypertension; systemic inflammation; inflammatory cytokines; cytokine storm; chemokines; white blood cells; granulocytes; lymphocytes; pigs; animal models; IL-6; IL-1beta



Copyright: © 2023 by the authors. Licensee MDPI, Basel, Switzerland. This article is an open access article distributed under the terms and conditions of the Creative Commons Attribution (CC BY) license (<https://creativecommons.org/licenses/by/4.0/>).

1. Introduction

The cytokine storm syndrome (CSS), a hyper-inflammation characterized by abnormally high levels of proinflammatory cytokines and other immune mediators in blood, is known to be a major contributor to the death of patients with severe COVID-19 [1–17]. Among others, high serum IL-6 and IL-1RA levels were found as independent risk factors for mortality from COVID-19 [18–23]. CSS is, however, not the only sign of bad prognosis in late-stage COVID-19. Another one is the association of neutrophilia with lymphopenia, manifested in a rise in neutrophil/lymphocyte ratio (NLR) [24,25], and yet another

is hemodynamic instability, including pulmonary hypertension [26–28] and/or systemic hypotension [29,30]. These symptoms can also arise in COVID-19 independent CSS [24–28]; thus, they are manifestations of the immune derangement, rather than direct consequences of the infection with SARS-CoV-2 virus.

A key piece of background information that provided rationale for this study was the fact that the hemodynamic derangement and WBC differential changes are also characteristic features of the pigs' response to i.v.-administered nanoparticles [31–35]. The experimental setup, referred to as porcine complement (C) activation-related pseudoallergy (CARPA) model, has been used for the screening of nanoparticulate drugs (nanomedicines) for potential immune reactivity, manifested in infusion reactions [31–35]. The model utilizes zymosan, a strong activator of the innate immune system, as a highly reproducible positive control. Notably, zymosan's robust pulmonary hypertensive and systemic hypotensive effects are observed essentially in all pigs regardless of whether they are responsive or not to the tested nanomedicines [32–34]. In the model, i.v. administration of a tiny amount of reactogenic nanoparticles induces prominent hemodynamic changes within minutes, including pulmonary hypertension, systemic hypotension, rise in heart rate, fall of cardiac output and ECG alterations. These transient changes may be associated with granulopenia, followed by reactive granulocytosis with or without thrombocytopenia, and skin alterations, such as flushing or a rash [31–35]. The above changes are easily measurable and are highly reproducible in different pigs, making the model uniquely useful for preclinical testing of acute allergic reactivity of nanoparticulate drugs or, in other words, the risk of anaphylactoid reactions [31–35]. This effect of zymosan in pigs, taken together with its capability to induce proinflammatory cytokines in murine models [36,37] and cultured human peripheral blood mononuclear cells (PBMCs) [38], led to the hypothesis that zymosan could be used to induce the above triad of prognostic endpoints of CSS in pigs, so that the use of the model can be extended to studying the mechanism and drug sensitivity of severe COVID-19 and other diseases involving CSS. Accordingly, the goal of the present experiments was to test if the adverse hemodynamic and hematological effects of zymosan could be associated with inflammatory cytokine release in pigs; if yes, the goal was to optimize the model to allow streamlined drug testing against CSS in severe COVID-19 and other diseases.

We observed that zymosan infusion triggered an acute pulmonary hypertension, followed by a prolonged and markedly increased neutrophil-to-lymphocyte ratio (NLR) in parallel with massive rise in IL-6, TNF-alpha, CCL-2, CXCL-10, and IL-1RA expression in blood, resembling COVID-19 associated severe cytokine storm syndrome.

2. Results

2.1. Early Hemodynamic, Hematological, and Immune Mediator Changes Caused by Low-Dose Bolus Injection of Zymosan

As the first step in pursuing the hypothesis delineated in the introduction, we reproduced the robust hemodynamic changes caused by a single bolus injection of 0.1 mg/kg zymosan in pigs. As shown in Figure 1, the cardiopulmonary reaction starts with a sudden rise in pulmonary arterial pressure (PAP) (A), fall of systemic arterial pressure (SAP) (C) and massive release of thromboxane B2 (TXB2) (G) exactly paralleling the PAP. The heart rate (HR, E) and blood cells (B, D, F) showed no major changes, although a small, statistically significant decline of granulocyte count was detectable (D). The SAP returned to baseline within 10 min, while it took longer for PAP and HR (up to 30 min, not shown) to return to near normal levels.

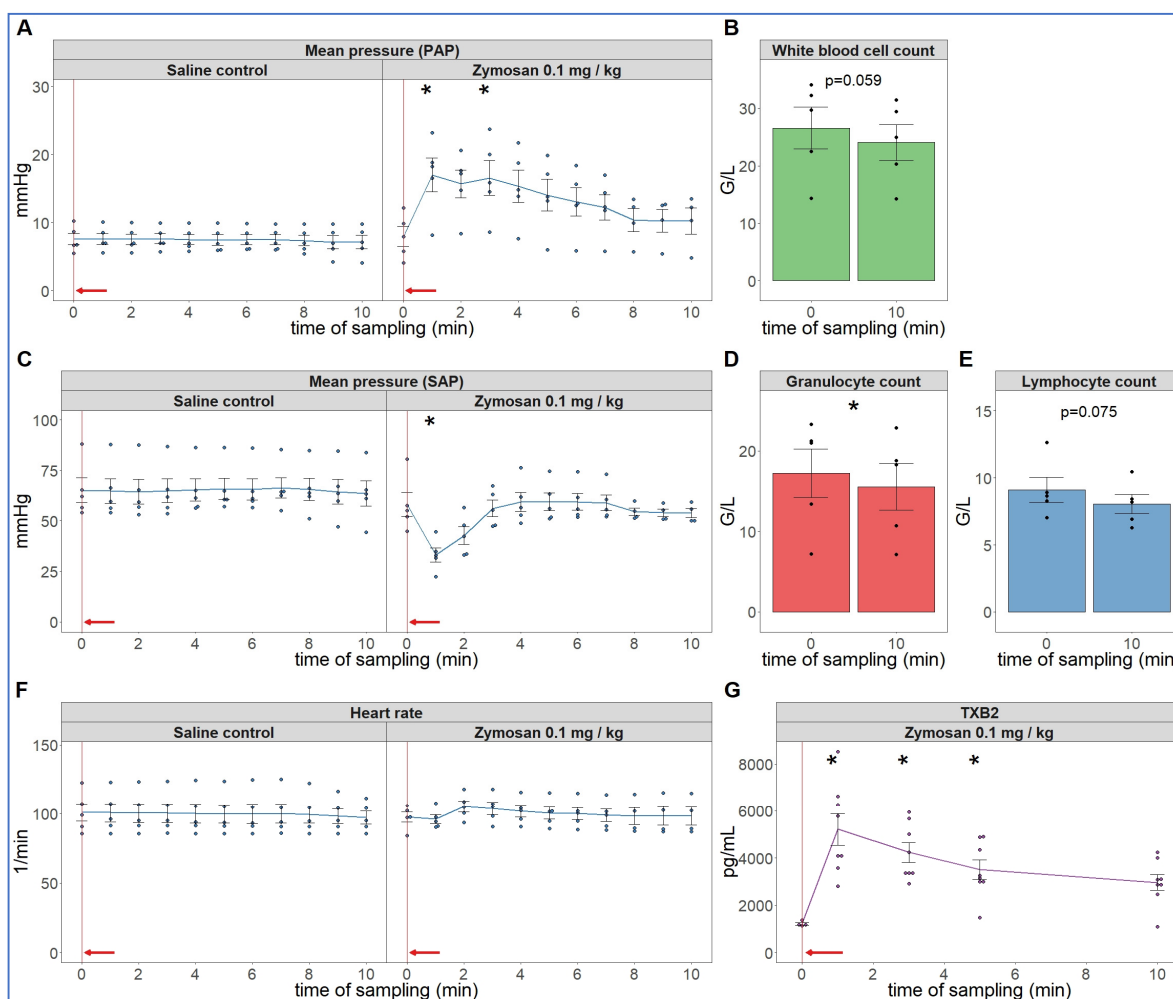


Figure 1. Physiological changes caused by bolus injection of 0.1 mg/kg zymosan in pigs. In (A,C,F) the PAP, SAP and HR were continuously recorded, and the coinciding values were averaged (\pm SEM) in four animals every minute over 10 min both before and after the zymosan injection. Zymosan administration is marked with red arrow. Blood white blood cell count (B), granulocytes (D) and lymphocytes (E) were counted in a coulter counter at 10 min after zymosan injection and were related to their respective baseline, i.e., the last blood collection before the zymosan injection (0 min). TXB2 increased 4-fold within a minute after zymosan administration (G). G/L means cell number $\times 10^6/L$, * $p < 0.05$ relative to respective baselines (0 min), determined using paired t -test.

2.2. Extended Follow-Up of Hemodynamic, Hematological, and Immune Mediator Changes Caused by High Dose Zymosan Infusion

Due to a lack of major neutrophilia, the mentioned symptom of late-stage COVID-19 that we were trying to identify, we increased the administered dose of zymosan 10-fold and gave it in infusion, rather than bolus. Because the hemodynamic monitoring is invasive, this experiment had to be terminated after 6.5 h (390 min) observation period. Figure 2 shows the hemodynamic changes after initiation of the zymosan infusion. Interestingly, the infusion was associated with maximal rise in PAP; after completing it, however, the pulmonary pressure normalized within 20 min. The SAP showed major fall during infusion and then slow return to normal in 1 of 4 animals; this is a measure that has proven to be very variable in all previous CARPA studies [39–44]. The heart rate and exhaled CO_2 , an indicator of pulmonary function, showed no significant differences. These data imply an immediate cardiovascular effect of zymosan, which can be explained with immediate TXA_2 release with entailing pulmonary vasoconstriction.

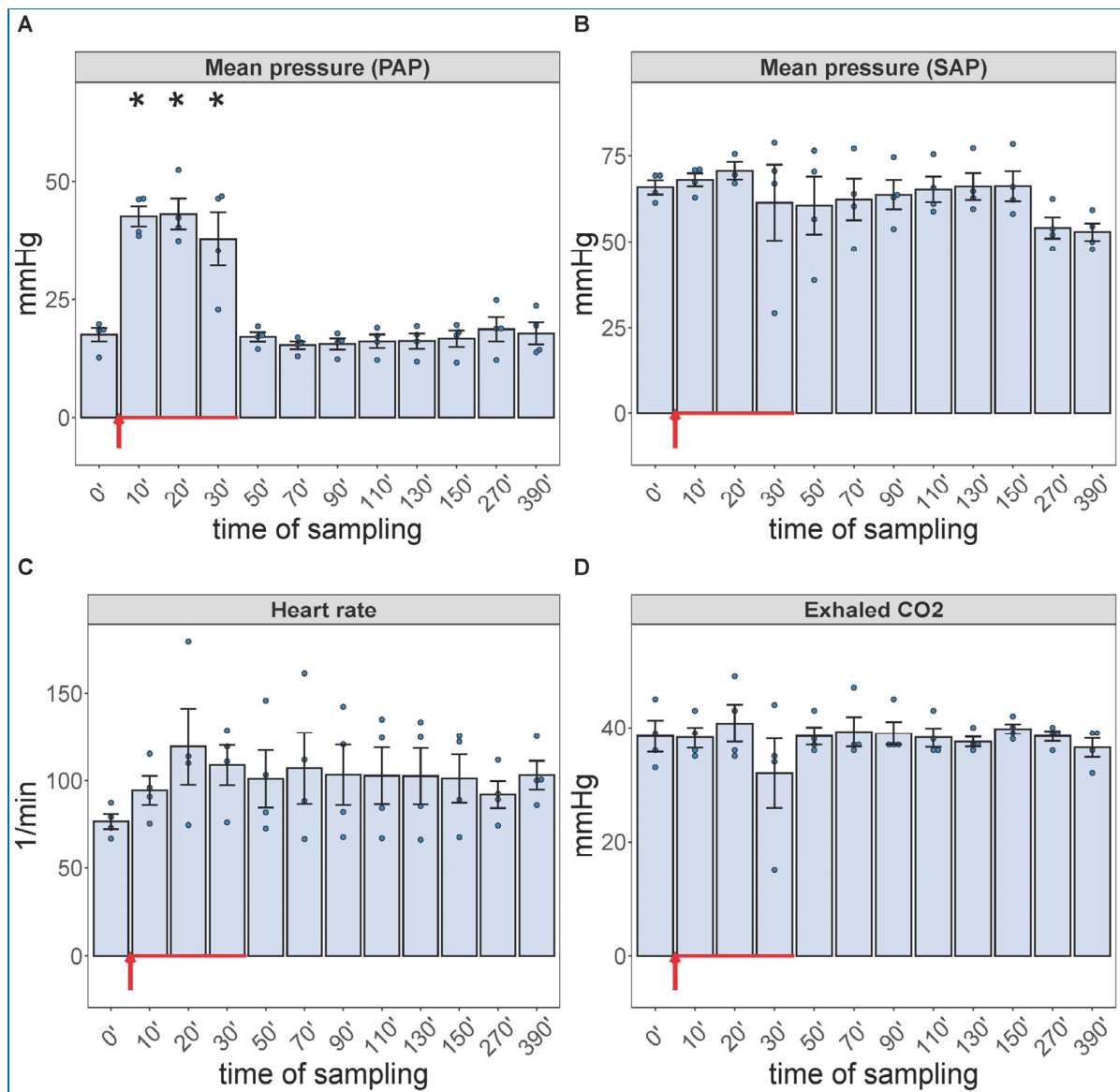


Figure 2. Physiological changes caused by infusion of 1.0 mg/kg zymosan in pigs. PAP (A), SAP (B), HR (C) and exhaled CO₂ (D) were continuously recorded up to 6.5 h, and the coinciding values at the indicated time points were averaged (\pm SEM) in four animals. Here, we show the blood pressure on absolute (mmHg) scale without the flat pre-injection background (Figure 1). The red arrow indicates zymosan administration. * $p < 0.05$ relative to respective baselines (0 min), determined using paired t -test.

Of particular importance regarding the hypothesis of this study, the blood cell changes did show the expected granulocytosis with lymphopenia, between about 1 and 6 h after starting the 30 min infusion. This effect is shown in Figure 3, together with data from five more pigs, which were not subjected to invasive blood pressure recording and, thus, were not sacrificed after 6.5 h. These animals were subjected to blood withdrawals for blood cell counting and cytokine analysis for up to 15 days, the results of which are presented below. The lack of significant changes in SAP, HR and exhaled CO₂ suggests that these processes, in case of slow access of zymosan to blood, may be independent of pulmonary hypertension.

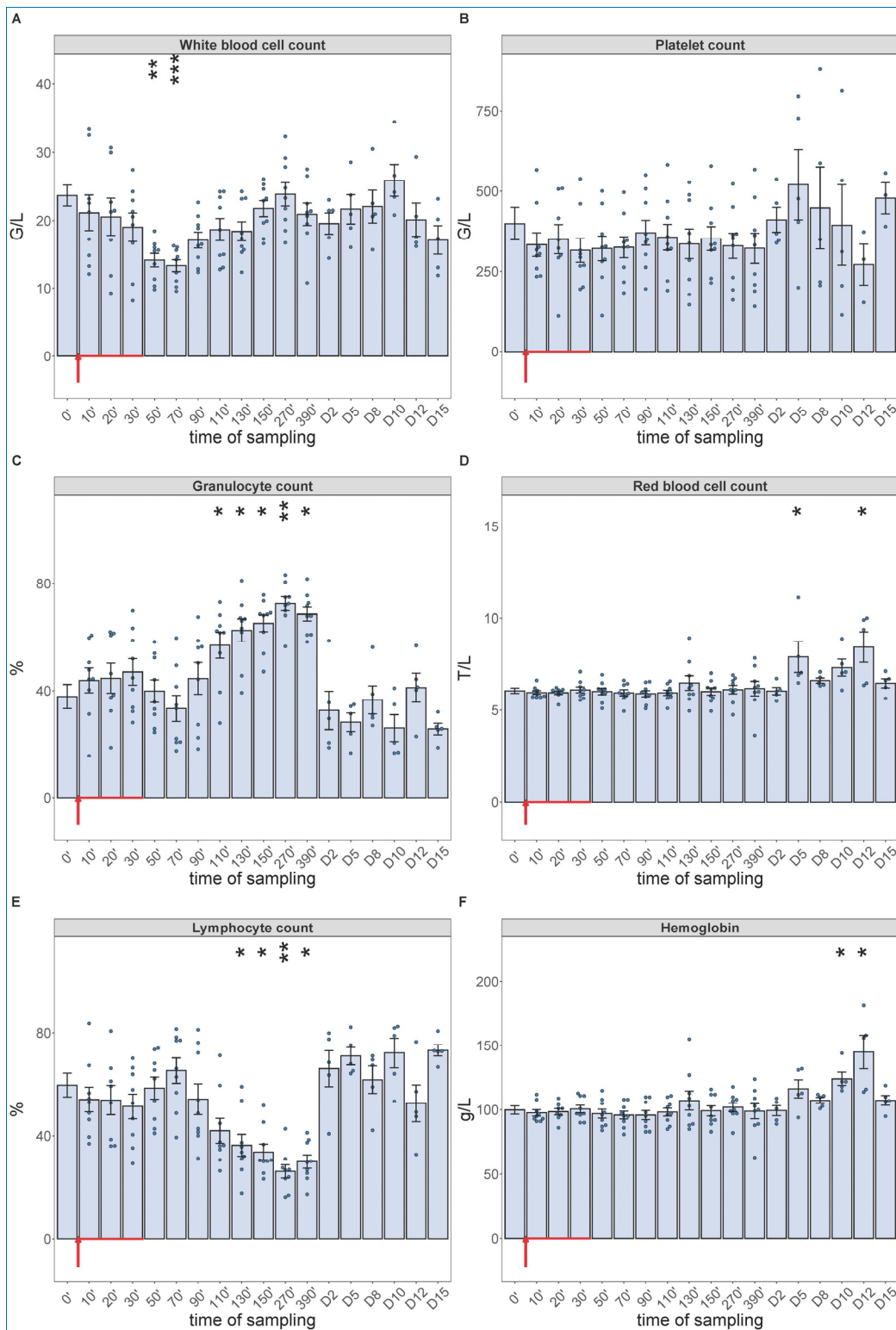


Figure 3. White blood cell count (A), platelet count (B), granulocyte % (C), RBC count (D), lymphocyte % (E), hemoglobin levels (F) at different sampling times. Zymosan administration is marked with red arrow. Until 390 min, the data have been merged from the 2nd ($n = 4$ pigs) and 3rd phase ($n = 5$ pigs) of the study, and their overlapping excludes a pro-inflammatory influence of hemodynamic monitoring (surgery). Kruskal–Wallis test with Dunn’s multiple comparisons post-hoc test, compared to respective baseline (0’) controls, * $p < 0.05$ vs. 0’; ** $p < 0.01$ vs. 0’; *** $p < 0.001$ vs. 0’.

2.3. Long-Term Follow-Up of Hematological, TXB2 and Cytokine Changes Caused by High Dose Zymosan Infusion

As shown in Figure 3, we observed a significant drop in WBC count around 1 h after the start of zymosan infusion (Figure 3A), which did not involve changes in neutrophil granulocyte/lymphocyte ratio (NLR, about 4/6) (Figure 3C,E). However, thenceforwards, while the WBC count returned to normal in about 3–4 h (Figure 3A), the NLR gradually rose up to 7/3, near 3–4-fold relative to the baseline ratio. In absence of absolute (total) increase or decrease in WBC count at the peak of NLR (Figure 3A,C,E), the above changes imply a relative leukocytosis with absolute lymphopenia, a shift in WBC differential in favor of the innate, nonspecific versus the acquired, specific antimicrobial immune response. The platelet count did not change over time (Figure 3B), and we did not measure consistent trends in RBC counts or blood hemoglobin levels either, although the numbers showed significant rises relative to baseline on some days (Figure 3D,F).

Regarding the cytokine changes, the PCR assay showed significant expression of CCL2 (Figure 4A), CXCL10 (B), IL-1RA (C) and IL-6 mRNAs in close parallelism with the changes in WBC differential, with peaks in the 90–270 min range. The relative mRNA expressions decreased in the above order, while in terms of speed, IL-6 mRNA had faster rise than those of the other 3 cytokines (peaking at already 90–110 min vs. 130–150 min). We also detected significant increases in IL-6 gene transcription in 2 of 5 animals on day 8 and 10, again (Figure 4D).

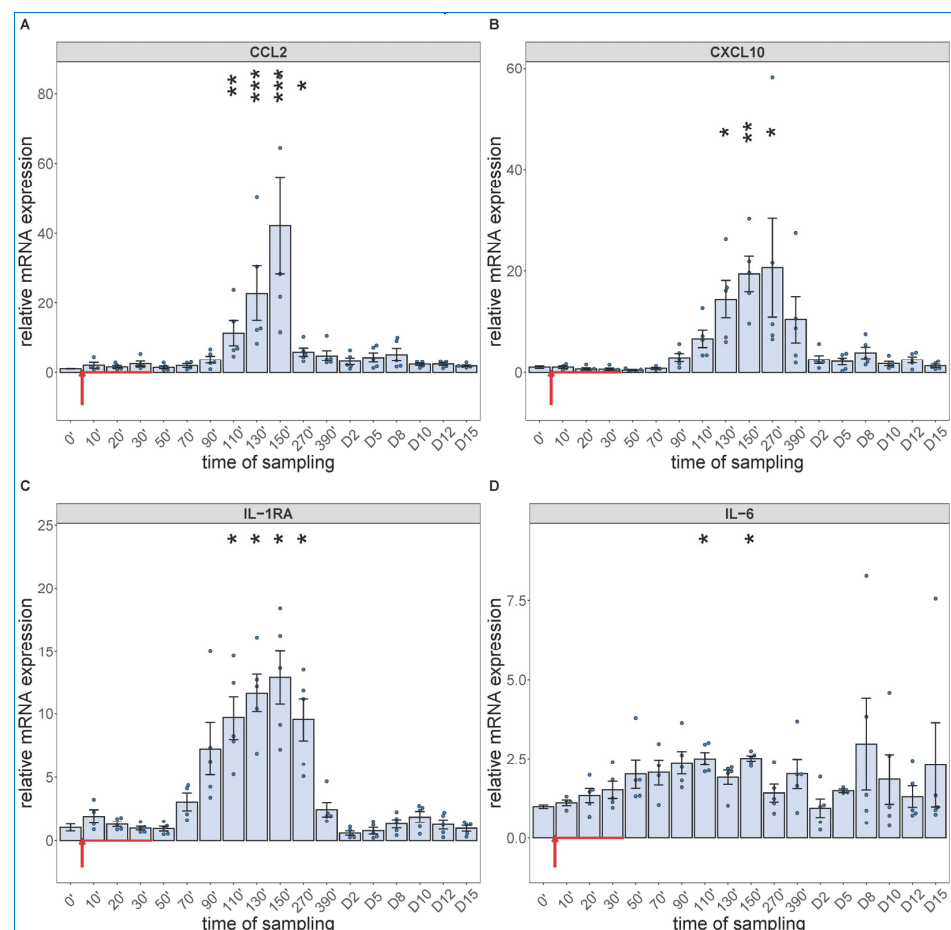


Figure 4. Gene expression of CCL2 (A), CXCL10 (B), IL-1RA (C) and IL-6 (D) were assessed from PBMCs isolated at different sampling times and normalized to 18S rRNA. Zymosan administration is marked with red arrow. Data are expressed as fold expression relative to a baseline control sample (0 min). Kruskal–Wallis test with Dunn’s multiple comparisons post-hoc test, compared to respective baseline (0’) controls, * $p < 0.05$ vs. 0’; ** $p < 0.01$ vs. 0’; *** $p < 0.001$ vs. 0’.

The cytokine protein assays performed for IL-6 and others (whose mRNA expression were not analyzed, i.e., TNF-alpha, IL-8 and IL-1beta) confirmed the early expression of IL-6 but showed the production of TNF- α to be even faster and more intense, peaking about 30 min earlier at about 10-fold higher concentration than IL-6 (Figure 5A,B). The concentrations of IL-8 and IL-1beta tended to be increased in some animals after day 10, with substantial individual variation (Figure 5C,D).

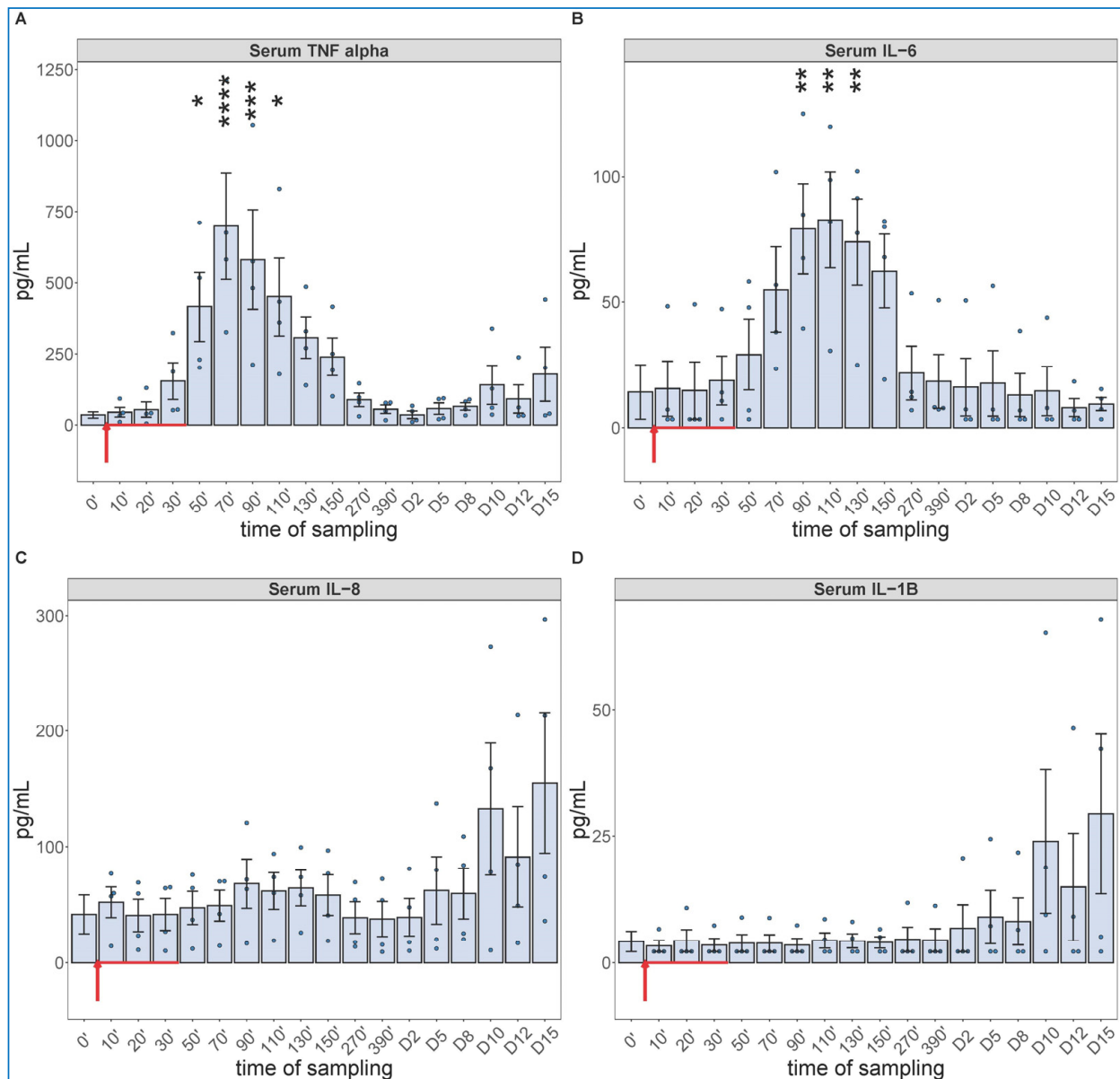


Figure 5. Serum TNF- α (A), IL-6 (B), IL-8 (C) and IL-1B (D) levels at different sampling times (ELISA). Zymosan administration is marked with red arrow. ANOVA, with Dunnett's multiple comparison test, compared to respective baseline (0') controls, * $p < 0.05$ vs. 0'; ** $p < 0.01$ vs. 0'; *** $p < 0.001$ vs. 0'; **** $p < 0.0001$ vs. 0'.

Comparing the kinetics of NLR changes with cytokine transcription or translation revealed overlays with all cytokines analyzed (Figure 6A–F), except IL-8 and IL-1beta, which did not show changes in the 30–270 min period (Figure 5C,D). Figure 6A–F also shows that the rise in NLR, which reflects a shift in cellular immune response towards innate defense, started after about 1 h and peaked at 5h (blue line in Figure 6A–F). The cytokines whose early rises and peaks consistently preceded these changes of NLR were

TNF- α and IL-6 (Figure 6A–C). In fact, for IL-6, we could show highly significant correlation between lymphopenia and IL-6 mRNA expression (Figure 7). Nevertheless, it would be premature to point to certain cytokines versus others as sole or most significant contributors to the blood cell changes, since there were also overlaps between the changes in NLR and expression of CCL2, IL-1RA and CXCL-10 genes (Figure 6D–F). Notably, we do not know the individual contribution of different cytokines to the blood cell changes. Thus, what can certainly be stated is that cytokine production correlated with the rise in NLR, which is consistent with the coincidence of NLR rise and CSS in severe COVID-19.

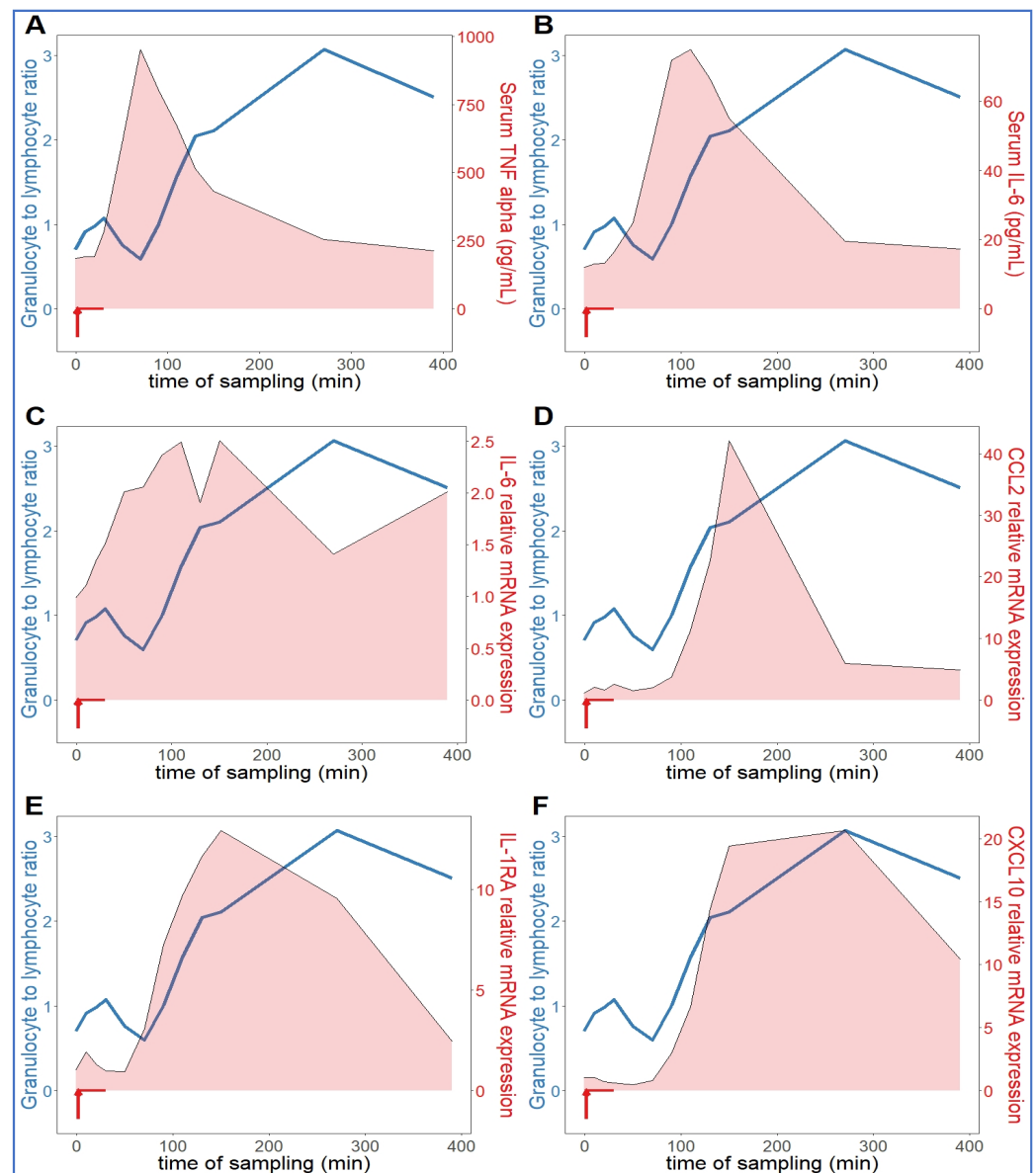


Figure 6. Relationship between serum cytokine levels and NLR. The NLR (neutrophil granulocyte-to-lymphocyte ratio) (blue line) increased continuously in an hour after zymosan administration, which was preceded by increased TNF-alpha (A) and IL-6 (B,C). The expression of CCL2 (D), IL-1RA (E) and CXCL10 (IP-10, (F)) genes proceeded in parallel with the rise in NLR ($n = 9$).

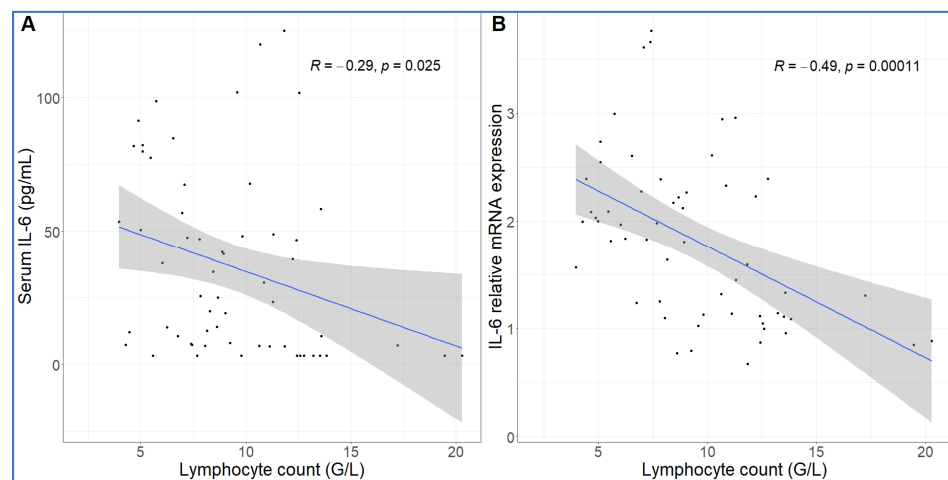


Figure 7. Correlation between IL-6 protein secretion and gene expression and absolute lymphocyte counts. The lymphopenia significantly correlated with increased IL-6 protein (A) and mRNA expression (B) over time. Linear regression.

3. Discussion

3.1. The Structure and Immune Effects of Zymosan

To help understand how a short infusion of yeast microparticles (zymosan) can reproduce three key manifestations of end-stage COVID-19 within 6 h, we summarize here the unique features of zymosan. It is extracted from the membrane of *Saccharomyces cerevisiae* and consists of mannosylated cell wall proteins and highly branched beta-glucans. The latter are D-glucose polymers linked by 1,3- and 1,6-beta-glycosidic-bonds. Zymosan is widely used in immunological studies as a powerful stimulator of innate humoral and cellular immunity. The chemical structures (Figure 8a–d) reveal little about zymosan’s real-life appearance (Figure 8e–i), i.e., 2–4 μm bean-shaped microparticles covered by knobs or bulges with extensions reminiscent of truncated bacterial pili [45,46].

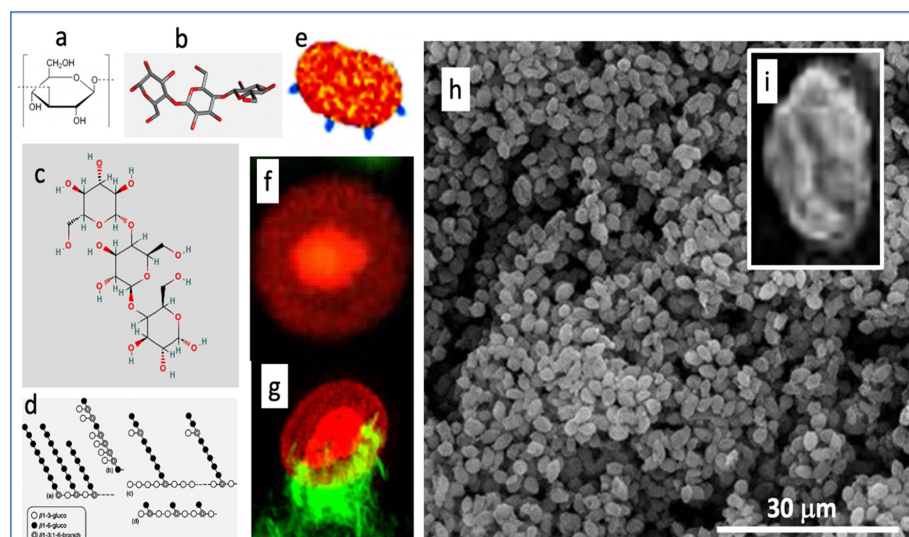


Figure 8. Various illustrations of zymosan. Panels (a–d) are chemical, graphical, and 3D-steric presentation of structure, (e) is an artistic visualization and (f–i) are electron microscopic and scanning electron microscopic images of zymosan. The corona in (f) is with a fluorescent dye conjugated to zymosan, and (g) is a zymosan particle undergoing phagocytosis, where the green fluorescing “claws” are macrophage pseudopods embracing the particle as first step of phagocytosis. The insert (i) is a particle zoomed in from (h). Free pictures from the internet and modified reproductions of figures in Ref. [47] with permission.

Zymosan was described as a potent activator of the complement system 81 years ago [48] and has been used for modeling phagocytosis [46]. Similarly to Toll-like receptor (TLR)-4 mediated LPS stimulation of NF- κ B in immune cells, zymosan stimulates the production of inflammatory cytokines via Toll-like receptors TLR-2 and TLR-6 [49,50]. Furthermore, zymosan activates another transmembrane signaling receptor, Dectin-1 [51–53], which collaborates with TLR-2 in NF- κ B mediated cytokine production [54,55]. Due to all these redundant pro-inflammatory stimuli, zymosan has been used in many inflammatory disease models in mice and rats, as listed in Table 1.

Table 1. Murine models of inflammatory diseases using zymosan as inflammation inducer.

Animal	Disease	Reference
mouse	irritable bowel syndrome	[56]
	T-cell-mediated autoimmune response	[57]
	allergy	[58]
	systemic inflammation	[59,60]
	arthritis	[61]
	sepsis	[62]
	air pouch model of inflammation	[63]
	multiple organ dysfunction syndrome (MODS)	[64]
	septic shock	[36]
	peritonitis	[65]
rat	arthritis	[66,67]
	air pouch model of inflammation	[68]
	chronic pelvic pain syndrome	[69]
	systemic inflammatory response syndrome (SIRS)	[70]
	peritonitis	[71]
	non-septic shock	[72]

3.2. Current Animal Models of CSS

Despite substantial efforts to develop effective pharmacotherapy against severe COVID-19, the standard of care today is based on traditional antibiotic and anti-inflammatory agents and some monoclonal antibodies, whose success is limited [73–76]. One contributing reason for the shortage of new, more specific, and effective drugs is the lack of an appropriate, widely accessible animal model of COVID-19 or CSS. Natural and genetically modified species used to model different aspects of COVID-19 include mice, ferrets, cats, dogs, pigs, and non-human primates [77–81]. The models described for CSS include the Staphylococcal superantigen mutant model in rabbits [82], the hemolytic transfusion model in mice [83], and the reactions of dogs to anti-CD28 mAb [84], primates to simian immunodeficiency virus [85], or pigs to a virulent African swine fever virus [86], yet another porcine model utilized LPS to induce CSS along with ARDS [87]. However, none of these models can recapitulate the sustained immunopathology of patients with severe COVID-19 or CSS. Moreover, the use of gene-modified animals and high-containment BSL3+ facility in the case of infectious virus are difficult to implement for high throughput drug testing in the pharmaceutical industry.

3.3. Molecular and Cellular Mechanisms of Zymosan's Multiple Effects

As to why it is possible in pigs to reproduce three unfavorable disease markers in severe COVID-19 with zymosan, a likely answer is that zymosan is a very strong, multi-valent stimulator of the innate immune system, a condition that also prevails in late stage COVID-19. Pigs, just as calves, sheep, goats, and some other species, are very sensitive to

innate immune stimulation [88]. These species have pulmonary intravascular macrophages (PIM cells) in their lungs' microcirculation, which firmly attach to the capillary endothelium via junction-like intercellular adhesion plaques [88]. The highly phagocytic and intense secretory PIM cells with direct access to blood are also close to the smooth muscle cell layer of blood vessels, making these animals' pulmonary arteries highly sensitive to the vasoactive mediators liberated upon encounter with, and phagocytic uptake of nanoparticles. These include TXA₂, a strong vasoconstrictor eicosanoid, which is the prime suspect in the hemodynamic changes caused by i.v. nanoparticles in pigs [88]. Zymosan can stimulate these macrophages via three independent pathways: one is via the anaphylatoxin (C3a, C5a) receptors, another is via TLR-2/6, and the third one is the Dectin-1 receptors [88]. These redundant activation pathways explain the high inter-animal reproducibility of hemodynamic changes caused by zymosan. Zymosan's exertion of its vasoactivity and pro-inflammatory cytokine-inducing effects via cells exposed to plasma is supported by the finding that the kinetics of liberation of TXB₂ and inflammatory cytokines in an in vitro peripheral blood mononuclear cell model of CSS [38] is very similar to those seen in pigs, namely immediate production of TXB₂ and slower release of cytokines on a time scale of hours [38].

Regarding the lymphopenia and its correlation with IL-6 gene expression (Figure 7), IL-6 is known to upregulate the pro-apoptotic Fas, resulting in the loss of mature lymphocytes [89]. High levels of IL-6 might also reduce lymphocyte count through inhibition of lymphopoiesis in the bone marrow [90]. The neutrophil granulocytosis, in turn, is a common sign of strong inflammation with cytokine release, a well-known disease marker. As for the roles of CCL2 (C-C motif chemokine ligand 2, also known as monocyte chemoattractant protein 1, MCP1) and CXCL (C-X-C motif chemokine ligand 10, also known as interferon gamma-induced protein 10, IP-10), we have no information in the literature that would suggest a direct role of these chemokines in rising the NLR.

3.4. The Utility of Porcine Zymosan-Induced CSS Model

The experimental procedures applied in this study represent relatively straightforward in vivo investigation of systemic flare-up of inflammatory processes in the body, a complex immune phenomenon, a feared end-stage of many severe diseases including COVID-19, viral infections [91], monoclonal antibody and CAR-T-cell therapies [92,93], acute respiratory disease syndrome [94], and multiorgan failure [94,95]. CSS has multiple manifestations, and the different models discussed above focus on different endpoints. In the present model, we have focused on three standard physiological parameters which have been reported as bad prognostic indicators in late-stage COVID-19: pulmonary hypertension, rise in NLR and cytokine release, which can be also common features of all CSS, regardless of cause. This choice of endpoints, taken together with the increasing appreciation of pigs, as an immune toxicology model [34], the inexpensive access to zymosan, the rapid (up to 6 h) experimentation, the avoidance of problematic interpretation of immune data in murine models, exotic animals or infectious viruses with need for BSL-3 facility, or sophisticated gene technology, suggests that the porcine zymosan-induced CSS model may provide a new tool to better understand and develop effective pharmacotherapies against CSS in general, and end-stage COVID-19, in particular.

3.5. Outlook for the Pharmaceutical Industry

Quoting from a recent review by Cron [73], "more than 2 years into the pandemic, almost 6 million people have died from COVID-19 worldwide. Many people who succumbed to the virus had CSS"; however, there is "no perfect therapy" for this disease [73]. There is a clear need for R&D of new drugs, drug combinations, and perhaps new treatment approaches against CSS. The preclinical testing of a large number of drug candidates at different doses and different combinations could certainly be streamlined by using an in vivo single-treatment, relatively short-duration, reproducible large animal model requiring only a small number of animals and using a reasonably simple endpoint. The porcine

model described in this study meets these conditions, and although the hemodynamic and cytokine changes were critical in realizing the relevance of the model for CSS and end-stage COVID-19, the third endpoint in this study, NLR, represents an automated routine laboratory blood assay that seems to be sufficiently quantitative and reproducible to provide a validatable disease marker without need for terminal surgery (for the PAP assay) or labor-intensive qPCR and polyplex ELISA tests of cytokines. In addition, the animals may be reused after a washout period, which may help in ethical and financial aspects.

4. Materials and Methods

4.1. Materials

Ficoll-Paque was obtained from GE Healthcare Bio-Sciences AB (Uppsala, Sweden). The porcine C3a kit was obtained from TECOMedical AG (Cat No: TE1078, Sissach, Switzerland). Zymosan, Dulbecco's phosphate-buffered saline (PBS) without Ca^{2+} / Mg^{2+} were from Sigma Chemical Co. (St. Louis, MO, USA). Pre-designed primers for IP10 (CXCL10, Assay cID: qSscCED0019399) and IL6 (Assay ID: qSscCED0014488) were purchased from BioRad laboratories (Herkules, CA, USA).

4.2. Animals

Landrace pigs were obtained from the Research Institute for Animal Breeding, Nutrition and Meat Science of the Hungarian University of Agriculture and Life Sciences (Herceghalom, Hungary). The study involved 13 female and castrated male pigs in the 22–32 kg size range. The experiments were approved by the Ethical Committee of Hungary for Animal Experimentation (permission numbers: PE/EA/843-7/2020 and conformed to the EU Directive 2010/63/EU and the Guide for the Care and Use of Laboratory Animals used by the US National Institutes of Health (NIH Publication No.85-23, revised 1996).

4.3. Anesthesia and Instrumentation

Animals were sedated with an intramuscular injection of 25 mg/kg ketamine (50 mg/mL, Gedeon Richter Plc. Budapest, Hungary) and 0.3 mg/kg midazolam (15 mg/3 mL, Kalceks AS, Riga, Latvia), and were carefully transported into the laboratory. Anesthesia was induced with a propofol bolus through an auricular vein. Airways were secured by inserting an endotracheal tube. Unless otherwise specified, animals were allowed to breathe spontaneously during the experiments. Controlled ventilation was applied in case of animals, where continuous measurement of hemodynamic parameters necessitated invasive surgical interventions. Surgery was done after povidone iodine (10%) disinfection of the skin. To measure the pulmonary arterial pressure (PAP), a Swan-Ganz catheter (Arrow AI-07124, 5 Fr. 110 cm, Teleflex, Morrisville, NC, USA) was introduced into the pulmonary artery via the right internal jugular vein. A Millar catheter (SPC-561, 6 Fr. Millar Instruments, Houston, TX, USA) was placed into the left femoral artery to record the systemic arterial pressure (SAP). Additional catheters were introduced into the left external jugular vein for drug administration, into the left femoral vein for venous blood sampling, and into the right common carotid artery for arterial blood gas analysis. The latter was executed with a Roche COBAS B221 benchtop analyzer (Roche Diagnostics, Rotkreuz ZG, Switzerland). Hemodynamic and ECG data were collected using instruments from Pulsion Medical Systems, and Powerlab, AD-Instruments (Castle Hill, Australia). Furthermore, end-tidal pCO_2 , ventilation rate and body temperature were also continuously measured, but they served no information beyond the measurements presented in this study and are therefore not shown.

4.4. Experimental Protocols in Different Stages

This study was performed in three stages to measure the acute (minutes) and subacute (hours to days) effects of zymosan in animals dedicated only to this study and in others where zymosan was used as control. In the latter case, we used animals where other treatments caused no or minimal physiological changes, and it could be ascertained that the

other treatments had no impact on zymosan's effects. In the first stage, five pigs were treated with bolus injection of 0.1 mg/kg zymosan, and the resultant hemodynamic, hematological and blood immune mediator changes were monitored or measured as described below. In the second stage 1 mg/kg zymosan was infused in four pigs over 30 min, and the same protocol was applied as in stage 1, except that the monitoring and serial blood sampling lasted for 6.5 h. In the third stage, five pigs were infused with 1 mg/kg zymosan, followed by blood withdrawals at 10, 20, 30, min, then in increasing times until 6.5 h, and then at 2–3 days intervals for 15 days.

4.5. Blood Assays

As described above, 10 mL of venous blood was drawn from the pigs at different times into EDTA containing vacuum blood collection tubes (K3EDTA Vacuette, Greiner Bio-One Hungary, Mosonmagyaróvár, Hungary). 0.5 mL of blood was aliquoted for use in an ABACUS Junior Vet hematology analyzer (Diatron, Budapest, Hungary) to measure the following parameters of blood cells: white blood cell (WBC), granulocyte (GR) and lymphocyte (LY), platelet (PLT), red blood cell (RBC) count and hemoglobin (Hgb) concentration. For measuring thromboxane B2 (TXB2), a stable metabolite of thromboxane A2 (TXA2), 4 µg indomethacin (diluted in 2 µL of 96% ethanol) was mixed with 2 mL of anticoagulated blood to prevent TXA2 release from WBC before centrifugation at 2000× *g*, for 4 min at 4 °C. Another 2 mL of anticoagulated blood was directly centrifuged using the same settings to separate the plasma. After centrifugation, the plasma samples were aliquoted, frozen, and stored at −70 °C until the TXB2 assay was performed as described in the kits' instructions. We used a commercially available ELISA kit (Cayman Chemicals, Ann Arbor, MI, USA) and an FLUOstar Omega microplate reader (BMG Labtech, Ortenberg, Germany).

4.6. Cytokine Measurements

Cytokine levels were measured in plasma samples derived from blood, which were taken in the previously discussed timepoints during and after zymosan infusion. The levels of IL-1beta, IL-6, IL-8 and TNF-alpha cytokines were determined using a high sensitivity 4-Plex Porcine Cytokine kit from Quansys Biosciences Inc. (Logan, UT, USA) according to the manufacturer's protocol. Briefly, samples and standards were diluted with the provided sample diluent in 1:1 ratio. An eight-point calibration curve (7 points, 1 blank) was prepared using freshly suspended calibrator and standard serial dilutions were prepared ranging 2.13–1550 pg/mL for IL-1beta, 2.47–1800 pg/mL for IL-6, 2.88–2100 pg/mL for IL-8 and 2.19–1600 pg/mL for TNF-alpha. In a final volume of 50 µL, the calibration curve standards and samples were pipetted on a Q-Plex™ Array 96-well plate. The plate was sealed, incubated for three hours, then washed with the provided wash solution, and the detection mix antibody solution was added. After 90 min incubation, the plate was washed; then, Streptavidin-HRP was added and incubated for another 20 min. After six final washes, the freshly prepared substrate solution was added and the plate was read immediately with 270 s exposure time using Imager LS by Quansys operated through Q-View Software (Quansys Biosciences, Logan, UT, USA), which was also used to evaluate the results. All samples and standards were measured in duplicate. All incubations were performed at room temperature (25 °C) on a shaker set to 500 rpm.

4.7. Isolation of PBMC and Quantitative RT-PCR

Peripheral blood mononuclear cells (PBMC) were isolated from 4 mL anticoagulated blood within 30 min at each experimental time point. Briefly, 2 mL blood was transferred into a 15 mL tube and diluted with 2 mL phosphate-buffer saline (PBS pH 7.4). In a new 15 mL tube, 3 mL Ficoll-Paque media (GE Healthcare, Chicago, IL, USA) was pipetted into the bottom and the diluted 4 mL blood sample was carefully layered on top, centrifuged for 30 min at 400× *g*. The upper plasma layer was removed, and the leukocyte layer was transferred into a new tube containing 6 mL PBS, washed and centrifuged. The PBMC pellet

was resuspended in 1 mL TriZol (Thermo Fisher Scientific, Waltham, MA, USA) and total RNA was extracted according to manufacturer's instructions. RNA pellet was resuspended in RNase-free water and the RNA concentration was determined photometrically on a NanoDrop microphotometer (Thermo Fisher). One microgram of RNA of each sample was reverse-transcribed with the high-capacity cDNA reverse transcription kit from Applied Biosystems (Applied Biosystems/Life Technologies, Carlsbad, CA, USA) using random primers in a final volume of 20 μ L. Quantitative real-time PCR reactions were performed on a Bio-Rad CFX96 thermal cycler (Bio-Rad Hungary, Budapest, Hungary) using the SensiFast SYBR Green PCR Master Mix (Thermo Fisher). The specificity and efficiency of each PCR reaction was confirmed with melting curve and standard curve analysis, respectively. Each sample was quantified in duplicate and normalized to the same sample's 18S rRNA (RN18S) expression. Mean expression values were calculated as fold expression relative to a baseline control sample using the $2^{-\Delta\Delta C_t}$ formula. Pre-designed primers for IP10 (CXCL10, Assay ID: qSscCED0019399) and IL6 (Assay ID: qSscCED0014488) were purchased from BioRad. Primer sequences for RN18S, IL1RA and CCL2 are shown in Table 2.

Table 2. Primer sequences for qPCR analysis.

Gene Symbol	Forward Primer	Reverse Primer
ssRN18S (NR_046261)	GACAAATCGCTCCACCAACT	CCTGCGGCTTAATTTGACTC
ssIL1RA (NM_214262)	CAAGCCTTCAGAATCTGGGATGTC	GGCTCAACAGGCACCACATC
ssCCL2 (NM_214214)	GAAGCAGTGATCTTCAAGAC	GGGCAAGTTAGAAGGAAATG

4.8. Statistical Analyses

All data are presented as mean \pm SD. Statistical analysis was performed using SPSS 10 (IBM, New York, NY, USA). Basic cardiopulmonary parameters were evaluated using paired *t*-test, while blood cell counts and PBMC gene expression values were evaluated using Kruskal–Wallis test and Dunn's post-hoc test for multiple comparisons. Serum cytokine protein levels were evaluated with ANOVA followed by Dunnett's multiple comparison test. Level of significance was set to $p < 0.05$ in each analysis.

Author Contributions: Conceptualization, J.S., T.R. and G.K.; methodology and formal analysis, G.K., B.A.B., G.T.K., T.M. and T.R.; investigation, T.B., B.A.B., G.V.N., T.M. and G.T.K.; resources, A.S., B.M. and T.R.; writing: J.S., G.K. and B.A.B.; writing—review and editing, J.S., G.K., B.A.B. and T.R.; supervision, T.R. and B.M.; project administration, B.M.; funding acquisition, A.S., T.R. and B.M. All authors have read and agreed to the published version of the manuscript.

Funding: This research was funded by the European Union Horizon 2020 projects 825828 (Expert) and 952520 (Biosafety) and National Research, Development, and Innovation Office (NKFIH) of Hungary (2020-1.1.6-JÖVŐ-2021-00013 and K134939 to T.R.). Open access funding was provided by Semmelweis University. G.K. was also supported by the Bolyai Scholarship of the Hungarian Academy of Sciences (BO/00304/20/5) and ÚNKP Bolyai+ Scholarship from the Hungarian Ministry of Innovation and Technology and National Research, Development, and Innovation Office (ÚNKP-22-5/202206201434KG). J.S. thanks the support by the Applied Materials and Nanotechnology Center of Excellence, Miskolc University, Miskolc.

Institutional Review Board Statement: The study was conducted in accordance with the Declaration of Helsinki, and the animal study protocol was approved by the Institutional and National Review Board/Ethics Committees, PE/EA/843-7/2020.

Data Availability Statement: Experimental data are available upon reasonable request to the corresponding author.

Acknowledgments: The expert technical support by Katalin Simay, Henriett Biró and Krisztina Fazekas are gratefully acknowledged.

Conflicts of Interest: The authors declare no conflict of interest.

References

1. Tang, Y.; Liu, J.; Zhang, D.; Xu, Z.; Ji, J.; Wen, C. Cytokine Storm in COVID-19: The Current Evidence and Treatment Strategies. *Front. Immunol.* **2020**, *11*, 1708. [\[CrossRef\]](#)
2. Pearce, L.; Davidson, S.M.; Yellon, D.M. The cytokine storm of COVID-19: A spotlight on prevention and protection. *Expert Opin. Ther. Targets* **2020**, *24*, 723–730. [\[CrossRef\]](#)
3. Sinha, P.; Matthay, M.A.; Calfee, C.S. Is a “Cytokine Storm” Relevant to COVID-19? *JAMA Intern. Med.* **2020**, *180*, 1152–1154. [\[CrossRef\]](#)
4. Buszko, M.; Park, J.H.; Verthelyi, D.; Sen, R.; Young, H.A.; Rosenberg, A.S. The dynamic changes in cytokine responses in COVID-19: A snapshot of the current state of knowledge. *Nat. Immunol.* **2020**, *21*, 1146–1151. [\[CrossRef\]](#)
5. Ragab, D.; Salah Eldin, H.; Taeimah, M.; Khattab, R.; Salem, R. The COVID-19 Cytokine Storm; What We Know So Far. *Front. Immunol.* **2020**, *11*, 1446. [\[CrossRef\]](#)
6. Iannaccone, G.; Scacciavillani, R.; Del Buono, M.G.; Camilli, M.; Ronco, C.; Lavie, C.J.; Abbate, A.; Crea, F.; Massetti, M.; Aspromonte, N. Weathering the Cytokine Storm in COVID-19: Therapeutic Implications. *Cardiorenal Med.* **2020**, *10*, 277–287. [\[CrossRef\]](#)
7. Del Valle, D.M.; Kim-Schulze, S.; Huang, H.-H.; Beckmann, N.D.; Nirenberg, S.; Wang, B.; Lavin, Y.; Swartz, T.H.; Madduri, D.; Stock, A.; et al. An inflammatory cytokine signature predicts COVID-19 severity and survival. *Nat. Med.* **2020**, *26*, 1636–1643. [\[CrossRef\]](#)
8. Peter, A.E.; Sandeep, B.V.; Rao, B.G.; Kalpana, V.L. Calming the Storm: Natural Immunosuppressants as Adjuvants to Target the Cytokine Storm in COVID-19. *Front. Pharmacol.* **2020**, *11*, 583777. [\[CrossRef\]](#)
9. Coperchini, F.; Chiovato, L.; Ricci, G.; Croce, L.; Magri, F.; Rotondi, M. The cytokine storm in COVID-19: Further advances in our understanding the role of specific chemokines involved. *Cytokine Growth Factor Rev.* **2021**, *58*, 82–91. [\[CrossRef\]](#)
10. Coperchini, F.; Chiovato, L.; Rotondi, M. Interleukin-6, CXCL10 and Infiltrating Macrophages in COVID-19-Related Cytokine Storm: Not One for All but All for One! *Front. Immunol.* **2021**, *12*, 668507. [\[CrossRef\]](#)
11. Hu, B.; Huang, S.; Yin, L. The cytokine storm and COVID-19. *J. Med. Virol.* **2021**, *93*, 250–256. [\[CrossRef\]](#)
12. Shen, W.X.; Luo, R.C.; Wang, J.Q.; Chen, Z.S. Features of Cytokine Storm Identified by Distinguishing Clinical Manifestations in COVID-19. *Front. Public Health* **2021**, *9*, 671788. [\[CrossRef\]](#)
13. Wright, D.J.M. Prevention of the cytokine storm in COVID-19. *Lancet Infect. Dis.* **2021**, *21*, 25–26. [\[CrossRef\]](#)
14. Machado, C.; Gonzalez-Quevedo, A. Hypoxemia and Cytokine Storm in COVID-19: Clinical Implications. *MEDICC Rev.* **2021**, *23*, 54–59.
15. Caricchio, R.; Gallucci, M.; Dass, C.; Zhang, X.; Gallucci, S.; Fleece, D.; Bromberg, M.; Criner, G.J. Preliminary predictive criteria for COVID-19 cytokine storm. *Ann. Rheum. Dis.* **2021**, *80*, 88–95. [\[CrossRef\]](#)
16. Cron, R.Q.; Caricchio, R.; Chatham, W.W. Calming the cytokine storm in COVID-19. *Nat. Med.* **2021**, *27*, 1674–1675. [\[CrossRef\]](#)
17. Morgulchik, N.; Athanasopoulou, F.; Chu, E.; Lam, Y.; Kamaly, N. Potential therapeutic approaches for targeted inhibition of inflammatory cytokines following COVID-19 infection-induced cytokine storm. *Interface Focus* **2022**, *12*, 20210006. [\[CrossRef\]](#)
18. Bai, Y.; Wang, E.; Zhao, S.; Li, J.; Zhu, Y.; Zhang, Y.; Cao, L.; Liu, H.; Dong, Y.; Wang, F.; et al. Implications of Laboratory Tests in Disease Grading and Death Risk Stratification of COVID-19: A Retrospective Study in Wuhan, China. *Front. Med.* **2021**, *8*, 629296. [\[CrossRef\]](#)
19. Wu, J.; Shen, J.; Han, Y.; Qiao, Q.; Dai, W.; He, B.; Pang, R.; Zhao, J.; Luo, T.; Guo, Y.; et al. Upregulated IL-6 Indicates a Poor COVID-19 Prognosis: A Call for Tocilizumab and Convalescent Plasma Treatment. *Front. Immunol.* **2021**, *12*, 598799. [\[CrossRef\]](#)
20. Galván-Román, J.M.; Rodríguez-García, S.C.; Roy-Vallejo, E.; Marcos-Jiménez, A.; Sánchez-Alonso, S.; Fernández-Díaz, C.; Alcaraz-Serna, A.; Mateu-Albero, T.; Rodríguez-Cortes, P.; Sánchez-Cerrillo, I.; et al. IL-6 serum levels predict severity and response to tocilizumab in COVID-19: An observational study. *J. Allergy Clin. Immunol.* **2021**, *147*, 72–80.e8. [\[CrossRef\]](#)
21. Smieszek, S.P.; Przychodzen, B.P.; Polymeropoulos, V.M.; Polymeropoulos, C.M.; Polymeropoulos, M.H. Assessing the potential correlation of polymorphisms in the IL6R with relative IL6 elevation in severely ill COVID-19 patients’. *Cytokine* **2021**, *148*, 155662. [\[CrossRef\]](#)
22. Garcia-Gasalla, M.; Berman-Riu, M.; Pons, J.; Rodríguez, A.; Iglesias, A.; Martínez-Pomar, N.; Llompert-Alabern, I.; Riera, M.; Beltrán, A.F.; Figueras-Castilla, A.; et al. Hyperinflammatory State and Low T1 Adaptive Immune Response in Severe and Critical Acute COVID-19 Patients. *Front. Med.* **2022**, *9*, 828678. [\[CrossRef\]](#)
23. Jakobs, K.; Reinshagen, L.; Puccini, M.; Friebe, J.; Wilde, A.-C.B.; Alsheik, A.; Rroku, A.; Landmesser, U.; Haghikia, A.; Kränkel, N.; et al. Disease Severity in Moderate-to-Severe COVID-19 Is Associated with Platelet Hyperreactivity and Innate Immune Activation. *Front. Immunol.* **2022**, *13*, 844701. [\[CrossRef\]](#)
24. Pirsalehi, A.; Salari, S.; Baghestani, A.; Vahidi, M.; Khave, L.J.; Akbari, M.E.; Bashash, D. Neutrophil-to-lymphocyte ratio (NLR) greater than 6.5 may reflect the progression of COVID-19 towards an unfavorable clinical outcome. *Iran. J. Microbiol.* **2020**, *12*, 466–474. [\[CrossRef\]](#)
25. Ciccullo, A.; Borghetti, A.; Verme, L.Z.D.; Tosoni, A.; Lombardi, F.; Garcovich, M.; Biscetti, F.; Montalto, M.; Cauda, R.; Di Giambenedetto, S. Neutrophil-to-lymphocyte ratio and clinical outcome in COVID-19: A report from the Italian front line. *Int. J. Antimicrob. Agents* **2020**, *56*, 106017. [\[CrossRef\]](#)

26. Tudoran, C.; Tudoran, M.; Lazureanu, V.E.; Marinescu, A.R.; Pop, G.N.; Pescariu, A.S.; Enache, A.; Cut, T.G. Evidence of Pulmonary Hypertension after SARS-CoV-2 Infection in Subjects without Previous Significant Cardiovascular Pathology. *J. Clin. Med.* **2021**, *10*, 199. [[CrossRef](#)]
27. Pagnesi, M.; Baldetti, L.; Beneduce, A.; Calvo, F.; Gramegna, M.; Pazzanese, V.; Ingallina, G.; Napolano, A.; Finazzi, R.; Ruggeri, A.; et al. Pulmonary hypertension and right ventricular involvement in hospitalised patients with COVID-19. *Heart* **2020**, *106*, 1324–1331. [[CrossRef](#)]
28. Khan, A.W.; Ullah, I.; Khan, K.S.; Tahir, M.J.; Masyeni, S.; Harapan, H. Pulmonary arterial hypertension post COVID-19: A sequela of SARS-CoV-2 infection? *Respir. Med. Case Rep.* **2021**, *33*, 101429. [[CrossRef](#)]
29. Sun, B.; Wang, H.; Lv, J.; Pei, H.; Bai, Z. Predictors of Mortality in Hospitalized COVID-19 Patients Complicated with Hypotension and Hypoxemia: A Retrospective Cohort Study. *Front. Med.* **2021**, *8*, 753035. [[CrossRef](#)]
30. Chen, Q.; Xu, L.; Dai, Y.; Ling, Y.; Mao, J.; Qian, J.; Zhu, W.; Di, W.; Ge, J. Cardiovascular manifestations in severe and critical patients with COVID-19. *Clin. Cardiol.* **2020**, *43*, 796–802. [[CrossRef](#)]
31. Szebeni, J.; Bedocs, P.; Csukas, D.; Rosivall, L.; Bunger, R.; Urbanics, R. A porcine model of complement-mediated infusion reactions to drug carrier nanosystems and other medicines. *Adv. Drug Deliv. Rev.* **2012**, *64*, 1706–1716. [[CrossRef](#)] [[PubMed](#)]
32. Urbanics, R.; Szebeni, J. Lessons learned from the porcine CARPA model: Constant and variable responses to different nanomedicines and administration protocols. *Eur. J. Nanomed.* **2015**, *7*, 219–231. [[CrossRef](#)]
33. Szebeni, J.; Bedöcs, P.; Dézsi, L.; Urbanics, R. A porcine model of complement activation-related pseudoallergy to nano-pharmaceuticals: Pros and cons of translation to a preclinical safety test. *Precis. Nanomed.* **2018**, *1*, 63–73. [[CrossRef](#)]
34. Szebeni, J.; Bawa, R. Human Clinical Relevance of the Porcine Model of Pseudoallergic Infusion Reactions. *Biomedicines* **2020**, *8*, 82. [[CrossRef](#)] [[PubMed](#)]
35. Patkó, Z.; Szebeni, J. Blood cell changes in complement activation-related pseudoallergy. *Eur. J. Nanomed.* **2015**, *7*, 233–244. [[CrossRef](#)]
36. von Asmuth, E.J.; Maessen, J.G.; van der Linden, C.J.; Buurman, W.A. Tumour necrosis factor alpha (TNF-alpha) and interleukin 6 in a zymosan-induced shock model. *Scand. J. Immunol.* **1990**, *32*, 313–319. [[CrossRef](#)]
37. Mogilski, S.; Kubacka, M.; Łażewska, D.; Więcek, M.; Głuch-Lutwin, M.; Tyszka-Czochara, M.; Bukowska-Strakova, K.; Filippek, B.; Kieć-Kononowicz, K. Aryl-1, 3, 5-triazine ligands of histamine H4 receptor attenuate inflammatory and nociceptive response to carrageen, zymosan and lipopolysaccharide. *Inflamm. Res.* **2017**, *66*, 79–95. [[CrossRef](#)] [[PubMed](#)]
38. Kozma, G.T.; Mészáros, T.; Bakos, T.; Hennies, M.; Bencze, D.; Uzonyi, B.; Györffy, B.; Cedrone, E.; Dobrovolskaia, M.A.; Józsi, M.; et al. Mini-Factor H Modulates Complement-Dependent IL-6 and IL-10 Release in an Immune Cell Culture (PBMC) Model: Potential Benefits against Cytokine Storm. *Front. Immunol.* **2021**, *12*, 642860. [[CrossRef](#)]
39. Fülöp, T.; Kozma, G.T.; Vashegyi, I.; Mészáros, T.; Rosivall, L.; Urbanics, R.; Storm, G.; Metselaar, J.M.; Szebeni, J. Liposome-induced hypersensitivity reactions: Risk reduction by design of safe infusion protocols in pigs. *J. Control. Release* **2019**, *309*, 333–338. [[CrossRef](#)]
40. Mészáros, T.; Kozma, G.T.; Shimizu, T.; Miyahara, K.; Turjeman, K.; Ishida, T.; Barenholz, Y.; Urbanics, R.; Szebeni, J. Involvement of complement activation in the pulmonary vasoactivity of polystyrene nanoparticles in pigs: Unique surface properties underlying alternative pathway activation and instant opsonization. *Int. J. Nanomed.* **2018**, *13*, 6345–6357. [[CrossRef](#)]
41. Jackman, J.A.; Meszaros, T.; Fulop, T.; Urbanics, R.; Szebeni, J.; Cho, N.J. Comparison of complement activation-related pseudoallergy in miniature and domestic pigs: Foundation of a validatable immune toxicity model. *Nanomedicine* **2016**, *12*, 933–943. [[CrossRef](#)]
42. Szebeni, J.; Bedöcs, P.; Rozsnyay, Z.; Weiszhar, Z.; Urbanics, R.; Rosivall, L.; Cohen, R.; Garbuzenko, O.; Báthori, G.; Tóth, M.; et al. Liposome-induced complement activation and related cardiopulmonary distress in pigs: Factors promoting reactogenicity of Doxil and AmBisome. *Nanomedicine* **2012**, *8*, 176–184. [[CrossRef](#)]
43. Szebeni, J.; Baranyi, L.; Savay, S.; Bodo, M.; Milosevits, J.; Alving, C.R.; Bünger, R. Complement activation-related cardiac anaphylaxis in pigs: Role of C5a anaphylatoxin and adenosine in liposome-induced abnormalities in ECG and heart function. *Am. J. Physiol. Heart Circ. Physiol.* **2006**, *290*, H1050–H1058. [[CrossRef](#)] [[PubMed](#)]
44. Szebeni, J.; Fontana, J.L.; Wassef, N.M.; Mongan, P.D.; Morse, D.S.; Dobbins, D.E.; Stahl, G.L.; Bünger, R.; Alving, C.R. Hemodynamic changes induced by liposomes and liposome-encapsulated hemoglobin in pigs: A model for pseudoallergic cardiopulmonary reactions to liposomes. Role of complement and inhibition by soluble CR1 and anti-C5a antibody. *Circulation* **1999**, *99*, 2302–2309. [[CrossRef](#)]
45. Di Carlo, F.J.; Fiore, J.V. On the composition of zymosan. *Science* **1958**, *127*, 756–757. [[CrossRef](#)]
46. Underhill, D.M. Macrophage recognition of zymosan particles. *J. Endotoxin Res.* **2003**, *9*, 176–180. [[CrossRef](#)] [[PubMed](#)]
47. Horsthemke, M.; Bachg, A.C.; Groll, K.; Moyzio, S.; Mütther, B.; Hemkemeyer, S.A.; Wedlich-Söldner, R.; Sixt, M.; Tacke, S.; Bähler, M.; et al. Multiple roles of filopodial dynamics in particle capture and phagocytosis and phenotypes of Cdc42 and Myo10 deletion. *J. Biol. Chem.* **2017**, *292*, 7258–7273. [[CrossRef](#)]
48. Pillemer, L.; Ecker, E.E. Anticomplementary factor in fresh yeast. *J. Biol. Chem.* **1941**, *137*, 139–142. [[CrossRef](#)]
49. Sato, M.; Sano, H.; Iwaki, D.; Kudo, K.; Konishi, M.; Takahashi, H.; Takahashi, T.; Imaizumi, H.; Asai, Y.; Kuroki, Y. Direct binding of Toll-like receptor 2 to zymosan, and zymosan-induced NF-kappa B activation and TNF-alpha secretion are down-regulated by lung collectin surfactant protein A. *J. Immunol.* **2003**, *171*, 417–425. [[CrossRef](#)]

50. Zhang, Y.; Liang, X.; Bao, X.; Xiao, W.; Chen, G. Toll-like receptor 4 (TLR4) inhibitors: Current research and prospective. *Eur. J. Med. Chem.* **2022**, *235*, 114291. [[CrossRef](#)] [[PubMed](#)]
51. Taylor, P.; Brown, G.; Reid, D.M.; Willment, J.; Martinez-Pomares, L.; Gordon, S.; Wong, S.Y.C. The beta-glucan receptor, dectin-1, is predominantly expressed on the surface of cells of the monocyte/macrophage and neutrophil lineages. *J. Immunol.* **2002**, *169*, 3876–3882. [[CrossRef](#)]
52. Brown, G.D.; Taylor, P.R.; Reid, D.M.; Willment, J.A.; Williams, D.L.; Martinez-Pomares, L.; Wong, S.Y.C.; Gordon, S. Dectin-1 is a major beta-glucan receptor on macrophages. *J. Exp. Med.* **2002**, *196*, 407–412. [[CrossRef](#)]
53. Brown, J.; O’Callaghan, C.A.; Marshall, A.S.; Gilbert, R.J.; Siebold, C.; Gordon, S.; Brown, G.D.; Jones, E.Y. Structure of the fungal beta-glucan-binding immune receptor dectin-1: Implications for function. *Protein Sci.* **2007**, *16*, 1042–1052. [[CrossRef](#)] [[PubMed](#)]
54. Brown, G.D. Dectin-1: A signalling non-TLR pattern-recognition receptor. *Nat. Rev. Immunol.* **2006**, *6*, 33–43. [[CrossRef](#)]
55. Goodridge, H.S.; Simmons, R.M.; Underhill, D.M. Dectin-1 stimulation by *Candida albicans* yeast or zymosan triggers NFAT activation in macrophages and dendritic cells. *J. Immunol.* **2007**, *178*, 3107–3115. [[CrossRef](#)] [[PubMed](#)]
56. Park, B.-K.; Chun, E.; Choi, J.J.; Shin, Y.; Kho, Y.T.; Oh, S.H.; Kim, S.Y.; Lee, T.H.; Kim, T.-W.; Shin, E.; et al. Administration of *Wasabia koreana* Ameliorates Irritable Bowel Syndrome-Like Symptoms in a Zymosan-Induced Mouse Model. *J. Med. Food* **2017**, *20*, 474–484. [[CrossRef](#)]
57. Park, S.; Park, D.-Y.; Kim, J.; Woo, K.I.; Kim, Y.-D.; Han, J.; Chung, T.-Y.; Cha, H.-S.; Lim, D.H. Enhanced orbital adipogenesis in a mouse model of T-cell-mediated autoimmunity, zymosan A-treated SKG mice: Implications for Graves’ ophthalmopathy. *Sci. Rep.* **2020**, *10*, 7329. [[CrossRef](#)]
58. Young, S.H.; Wolfarth, M.G.; Roberts, J.R.; Kashon, M.L.; Antonini, J.M. Adjuvant effect of zymosan after pulmonary treatment in a mouse ovalbumin allergy model. *Exp. Lung Res.* **2013**, *39*, 48–57. [[CrossRef](#)] [[PubMed](#)]
59. Rahat, M.A.; Brod, V.; Amit-Cohen, B.C.; Henig, O.; Younis, S.; Bitterman, H. Oxygen Mitigates the Inflammatory Response in a Model of Hemorrhage and Zymosan-Induced Inflammation. *Shock* **2016**, *45*, 198–208. [[CrossRef](#)]
60. Sugimoto, Y.; Endo, D.; Aratani, Y. Mice Deficient in NOX2 Display Severe Thymic Atrophy, Lymphopenia, and Reduced Lymphopoiesis in a Zymosan-Induced Model of Systemic Inflammation. *Inflammation* **2021**, *44*, 371–382. [[CrossRef](#)]
61. Frasnelli, M.E.; Tarussio, D.; Chobaz-Peclat, V.; Busso, N.; So, A. TLR2 modulates inflammation in zymosan-induced arthritis in mice. *Arthritis Res. Ther.* **2005**, *7*, R370–R379. [[CrossRef](#)]
62. Xie, K.; Yu, Y.; Zhang, Z.; Liu, W.; Pei, Y.; Xiong, L.; Hou, L.; Wang, G. Hydrogen gas improves survival rate and organ damage in zymosan-induced generalized inflammation model. *Shock* **2010**, *34*, 495–501. [[CrossRef](#)]
63. Yoon, S.-Y.; Kwon, Y.-B.; Kim, H.-W.; Roh, D.-H.; Kang, S.-Y.; Kim, C.-Y.; Han, H.J.; Kim, K.-W.; Yang, I.-S.; Beitz, A.J.; et al. Intrathecal neostigmine reduces the zymosan-induced inflammatory response in a mouse air pouch model via adrenomedullary activity: Involvement of spinal muscarinic type 2 receptors. *Neuropharmacology* **2005**, *49*, 275–282. [[CrossRef](#)]
64. Volman, T.J.; Goris, R.J.; Hendriks, T. Pentoxifylline does not improve outcome in a murine model for the multiple-organ dysfunction syndrome. *Intensive Care Med.* **2005**, *31*, 701–708. [[CrossRef](#)]
65. Mizuno, M.; Ito, Y.; Hepburn, N.; Mizuno, T.; Noda, Y.; Yuzawa, Y.; Harris, C.L.; Morgan, B.P.; Matsuo, S. Zymosan, but not lipopolysaccharide, triggers severe and progressive peritoneal injury accompanied by complement activation in a rat peritonitis model. *J. Immunol.* **2009**, *183*, 1403–1412. [[CrossRef](#)]
66. Chaves, H.V.; de Albuquerque Ribeiro, R.; de Souza, A.M.B.; e Silva, A.A.R.; Gomes, A.S.; Vale, M.L.; Bezerra, M.M.; de Castro Brito, G.A. Experimental model of zymosan-induced arthritis in the rat temporomandibular joint: Role of nitric oxide and neutrophils. *J. Biomed. Biotechnol.* **2011**, *2011*, 707985. [[CrossRef](#)] [[PubMed](#)]
67. Dief, A.E.; Mostafa, D.K.; Sharara, G.M.; Zeitoun, T.H. Hydrogen sulfide releasing naproxen offers better anti-inflammatory and chondroprotective effect relative to naproxen in a rat model of zymosan induced arthritis. *Eur. Rev. Med. Pharmacol. Sci.* **2015**, *19*, 1537–1546. [[PubMed](#)]
68. Paya, M.; Terencio, M.C.; Ferrandiz, M.L.; Alcaraz, M.J. Involvement of secretory phospholipase A2 activity in the zymosan rat air pouch model of inflammation. *Br. J. Pharmacol.* **1996**, *117*, 1773–1779. [[CrossRef](#)]
69. Aydogdu, O.; Gocun, P.U.; Aronsson, P.; Carlsson, T.; Winder, M. Prostate-to-bladder cross-sensitization in a model of zymosan-induced chronic pelvic pain syndrome in rats. *Prostate* **2021**, *81*, 252–260. [[CrossRef](#)]
70. Lu, Q.Y.; Zhou, Y.Y.; Wang, J.B.; Wang, L.; Meng, L.; Weng, J.K.; Yu, B.; Quan, S. [Preparation of rat model of systemic inflammatory response syndrome induced by zymosan]. *Zhejiang Da Xue Xue Bao Yi Xue Ban* **2011**, *40*, 641–646. [[PubMed](#)]
71. Yamamoto, S.; Kubota, Y.; Tsuji, K.; Yanagitani, K.; Takaoka, M.; Kin, H.; Ogura, M.; Inoue, K. Effect of obstructive jaundice on neutrophil chemotactic activity: An in vivo assessment in zymosan-induced peritonitis model in rats. *J. Gastroenterol. Hepatol.* **1998**, *13*, 405–411. [[CrossRef](#)] [[PubMed](#)]
72. Unsal, D.; Kacan, M.; Temiz-Resitoglu, M.; Guden, D.; Korkmaz, B.; Sari, A.; Buharalioglu, C.; Yildirim-Yaroglu, H.; Tamer-Gumus, L.; Tunctan, B.; et al. The role of Syk/IkB-alpha/NF-kB pathway activation in the reversal effect of BAY 61-3606, a selective Syk inhibitor, on hypotension and inflammation in a rat model of zymosan-induced non-septic shock. *Clin. Exp. Pharmacol. Physiol.* **2018**, *45*, 155–165. [[CrossRef](#)] [[PubMed](#)]
73. Cron, R.Q. No perfect therapy for the imperfect COVID-19 cytokine storm. *Lancet Rheumatol.* **2022**, *4*, e308–e310. [[CrossRef](#)]
74. Abusalah, M.A.H.; Khalifa, M.; Al-Hatamleh, M.A.I.; Jarrar, M.; Mohamud, R.; Chan, Y.Y. Nucleic Acid-Based COVID-19 Therapy Targeting Cytokine Storms: Strategies to Quell the Storm. *J. Pers. Med.* **2022**, *12*, 386. [[CrossRef](#)]

75. Zanza, C.; Romenskaya, T.; Manetti, A.C.; Franceschi, F.; La Russa, R.; Bertozzi, G.; Maiese, A.; Savioli, G.; Volonnino, G.; Longhitano, Y. Cytokine Storm in COVID-19: Immunopathogenesis and Therapy. *Medicina* **2022**, *58*, 144. [[CrossRef](#)] [[PubMed](#)]
76. Jiang, Y.; Rubin, L.; Peng, T.; Liu, L.; Xing, X.; Lazarovici, P.; Zheng, W. Cytokine storm in COVID-19: From viral infection to immune responses, diagnosis and therapy. *Int. J. Biol. Sci.* **2022**, *18*, 459–472. [[CrossRef](#)] [[PubMed](#)]
77. Zhao, S.; Fan, J.; Liu, E. Animal Models for COVID-19 Therapeutic Development: Where We Are and Where We Need to Go. *Front. Microbiol.* **2022**, *13*, 907406. [[CrossRef](#)]
78. Sefik, E.; Israelow, B.; Mirza, H.; Zhao, J.; Qu, R.; Kaffe, E.; Song, E.; Halene, S.; Meffre, E.; Kluger, Y.; et al. A humanized mouse model of chronic COVID-19. *Nat. Biotechnol.* **2022**, *40*, 906–920. [[CrossRef](#)]
79. Fan, C.; Wu, Y.; Rui, X.; Yang, Y.; Ling, C.; Liu, S.; Liu, S.; Wang, Y. Animal models for COVID-19: Advances, gaps and perspectives. *Signal Transduct. Target. Ther.* **2022**, *7*, 220. [[CrossRef](#)]
80. Park, J.G.; Pino, P.A.; Akhter, A.; Alvarez, X.; Torrelles, J.B.; Martinez-Sobrido, L. Animal Models of COVID-19: Transgenic Mouse Model. *Methods Mol. Biol.* **2022**, *2452*, 259–289.
81. Singh, D.K.; Cole, J.; Escobedo, R.A.; Alfson, K.J.; Singh, B.; Lee, T.-H.; Alvarez, X.; Ganatra, S.R.; Carrion, J.R.; Kaushal, D. Animal Models of COVID-19: Nonhuman Primates. *Methods Mol. Biol.* **2022**, *2452*, 227–258. [[PubMed](#)]
82. Stich, N.; Waclavicek, M.; Model, N.; Eibl, M.M. Staphylococcal superantigen (TSST-1) mutant analysis reveals that t cell activation is required for biological effects in the rabbit including the cytokine storm. *Toxins* **2010**, *2*, 2272–2288. [[CrossRef](#)] [[PubMed](#)]
83. Hod, E.A.; Cadwell, C.M.; Liepkalns, J.S.; Zimring, J.C.; Sokol, S.A.; Schirmer, D.A.; Jhang, J.; Spitalnik, S.L. Cytokine storm in a mouse model of IgG-mediated hemolytic transfusion reactions. *Blood* **2008**, *112*, 891–894. [[CrossRef](#)] [[PubMed](#)]
84. Rosinski, S.L.; Storb, R.; Strong, R.K.; Sale, G.E.; Stone, D.M.; Gewe, M.M.; Friend, D.J.; Abrams, V.K.; Randolph-Habecker, J.; Graves, S.S. Anti-CD28 Antibody-Initiated Cytokine Storm in Canines. *Transplant. Direct* **2015**, *1*, 1–11. [[CrossRef](#)]
85. Keating, S.M.; Heitman, J.W.; Wu, S.; Deng, X.; Stacey, A.R.; Zahn, R.C.; de la Rosa, M.; Finstad, S.L.; Lifson, J.D.; Piatak, M.; et al. Magnitude and Quality of Cytokine and Chemokine Storm during Acute Infection Distinguish Nonprogressive and Progressive Simian Immunodeficiency Virus Infections of Nonhuman Primates. *J. Virol.* **2016**, *90*, 10339–10350. [[CrossRef](#)]
86. Wang, S.; Zhang, J.; Zhang, Y.; Yang, J.; Wang, L.; Qi, Y.; Han, X.; Zhou, X.; Miao, F.; Chen, T.; et al. Cytokine Storm in Domestic Pigs Induced by Infection of Virulent African Swine Fever Virus. *Front. Vet. Sci.* **2020**, *7*, 601641. [[CrossRef](#)]
87. Xu, X.; Jia, C.; Luo, S.; Li, Y.; Xiao, F.; Dai, H.; Wang, C. Effect of HA330 resin-directed hemoadsorption on a porcine acute respiratory distress syndrome model. *Ann. Intensive Care* **2017**, *7*, 84. [[CrossRef](#)]
88. Csukas, D.; Urbanics, R.; Weber, G.; Rosivall, L.; Szebeni, J. Pulmonary intravascular macrophages: Prime suspects as cellular mediators of porcine CARPA. *Eur. J. Nanomed.* **2015**, *7*, 27–36. [[CrossRef](#)]
89. Choi, C.; Park, J.Y.; Lee, J.; Lim, J.-H.; Shin, E.-C.; Ahn, Y.S.; Kim, C.-H.; Kim, S.-J.; Kim, J.-D.; Choi, I.S.; et al. Fas ligand and Fas are expressed constitutively in human astrocytes and the expression increases with IL-1, IL-6, TNF-alpha, or IFN-gamma. *J. Immunol.* **1999**, *162*, 1889–1895. [[CrossRef](#)]
90. Maeda, K.; Baba, Y.; Nagai, Y.; Miyazaki, K.; Malykhin, A.; Nakamura, K.; Kincade, P.W.; Sakaguchi, N.; Coggeshall, K.M. IL-6 blocks a discrete early step in lymphopoiesis. *Blood* **2005**, *106*, 879–885. [[CrossRef](#)]
91. Sordillo, P.P.; Helson, L. Curcumin suppression of cytokine release and cytokine storm. A potential therapy for patients with Ebola and other severe viral infections. *In Vivo* **2015**, *29*, 1–4. [[PubMed](#)]
92. Lee, D.W.; A Gardner, R.; Porter, D.L.; Louis, C.U.; Ahmed, N.; Jensen, M.C.; Grupp, S.A.; Mackall, C.L. Current concepts in the diagnosis and management of cytokine release syndrome. *Blood* **2014**, *124*, 188–195. [[CrossRef](#)]
93. Kroschinsky, F.; Stölzel, F.; von Bonin, S.; Beutel, G.; Kochanek, M.; Kiehl, M.; Schellongowski, S.; on behalf of the Intensive Care in Hematological; Oncological Patients (iCHOP) Collaborative Group. New drugs, new toxicities: Severe side effects of modern targeted and immunotherapy of cancer and their management. *Crit. Care* **2017**, *21*, 89. [[CrossRef](#)] [[PubMed](#)]
94. Neuhofer, H. Actions and interactions of mediator systems and mediators in the pathogenesis of ARDS and multiorgan failure. *Acta Anaesthesiol. Scand. Suppl.* **1991**, *95*, 7–13. [[CrossRef](#)] [[PubMed](#)]
95. Kollias, G.; Douni, E.; Kassiotis, G.; Kontoyiannis, D. On the role of tumor necrosis factor and receptors in models of multiorgan failure, rheumatoid arthritis, multiple sclerosis and inflammatory bowel disease. *Immunol. Rev.* **1999**, *169*, 175–194. [[CrossRef](#)] [[PubMed](#)]

Disclaimer/Publisher’s Note: The statements, opinions and data contained in all publications are solely those of the individual author(s) and contributor(s) and not of MDPI and/or the editor(s). MDPI and/or the editor(s) disclaim responsibility for any injury to people or property resulting from any ideas, methods, instructions or products referred to in the content.